ARTICLE

Direct Patterning of TiO_2 Using Step-and-Flash Imprint Lithography

Ramakrishnan Ganesan,* Jarrett Dumond, Mohammad S. M. Saifullah,* Su Hui Lim, Hazrat Hussain,† and Hong Yee Low

Institute of Materials Research and Engineering, A*STAR (Agency for Science, Technology and Research), 3 Research Link, Singapore 117602, Republic of Singapore. †Present address: Department of Chemistry, University College of Sciences (Shankar), Abdul Wali Khan University, Mardan 23200 (Khyber Pakhtunkhwa), Republic of Pakistan.

ABSTRACT

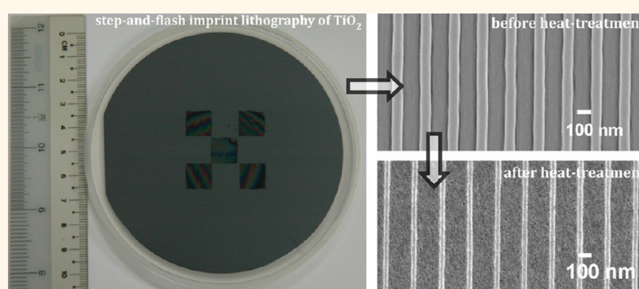

Although step-and-flash imprint lithography, or S-FIL, has brought about tremendous advancement in wafer-scale fabrication of sub-100 nm features of photopolymerizable organic and organo-silicon-based resists, it has not been successful in direct patterning of inorganic materials such as oxides because of the difficulties associated with resist formulation and its dispensing. In this paper, we demonstrate the proof-of-concept S-FIL of titanium dioxide (TiO_2) carried by an acrylate-based formulation containing an allyl-functionalized titanium complex. The prepolymer formulation contains 48 wt % metal precursor, but it exhibits low enough viscosity (∼5 mPa·s) to be dispensed by an automatic dispensing system, adheres and spreads well on the substrate, is insensitive to pattern density variations, and rapidly polymerizes when exposed to broadband UV radiation to give a yield close to 95%. Five fields, each measuring 1 cm × 1 cm, consisting of 100 nm gratings were successively imprinted. Heat-treatment of the patterned structures at 450 °C resulted in the loss of organics and their subsequent shrinkage without the loss of integrity or aspect ratio and converted them to TiO_2 anatase nanostructures as small as 30 nm wide. With this approach, wafer-scale direct patterning of functional oxides on a sub-100 nm scale using S-FIL can become a distinct possibility.

KEYWORDS: step-and-flash nanoimprint lithography · metal oxides · nanolithography · nanofabrication

Owing to its outstanding material properties, titanium dioxide (TiO_2) has gained enormous potential for technological applications in diverse areas such as solar cells,[1] optical waveguides,[2] photocatalysis,[3] and sensors.[4] For many of these applications, it is preferable to have TiO_2 in a patterned form to improve the material property. Unsurprisingly, TiO_2 is perhaps the most extensively patterned oxide, with several patterning techniques such as optical lithography,[5] electron beam lithography,[6] direct write assembly,[7] two-photon lithography,[8] electrohydrodynamic patterning,[9] proton beam writing,[10] and nanoimprint lithography (NIL) have been used to pattern it.[11,12] Out of these techniques, NIL has emerged as a viable alternative to traditional lithography techniques because of its simplicity, versatility, low-cost, high-resolution, and potential for achieving high throughput. This technique not only enables patterning of resists but also is capable of imprinting functional device structures that can lead to extensive applications in photonics, data storage, and biology.[13−15] Among the imprint-based lithographic technologies, thermal NIL and UV-NIL are the two techniques capable of replicating sub-10 nm features.[16−19] The fundamental principle of these imprint-based techniques is that a rigid template or mold is pressed into a deformable material or liquid resist to form a pattern. The material is then hardened so that when the mold is removed, the topography of the mold is transferred into the material.

In thermal NIL, the most versatile of imprint techniques, mold patterns are replicated into a thermoplastic material by heating the polymer above its glass transition temperature and applying pressure on the mold. A variant of this technique involves a liquid imprint resist, which can be made to undergo *in situ* free radical polymerization by simultaneous heating and applying pressure to the template.[11,20] Thermal NIL has been used extensively to imprint a wide range of materials such as thermoplastics, thermosets, sol−gel films, and metalorganic materials.[21−30] Although thermal NIL has demonstrated high-resolution patterns, this technique essentially is a batch process involving temperature cycling at high pressure to pattern the resist. Such a process not only results in lowering of the template life but also leads to

* Address correspondence to ganesanr@imre.a-star.edu.sg, saifullahm@imre.a-star.edu.sg.

Received for review November 14, 2011 and accepted January 9, 2012.

Published online January 09, 2012
10.1021/nn204405k

© 2012 American Chemical Society

reduced throughput and improper overlay of device layers due to differences in coefficients of thermal expansion of the resist, substrate, and template. These disadvantages are circumvented by UV-NIL, which is performed at low pressure and at room temperature. This method does not require temperature cycling and, hence, leads to higher throughput than that in thermal NIL. Furthermore, the transparency of the template offers the possibility for easy optical and high-precision alignment. This advantage is exploited in step-and-flash imprint lithography (S-FIL), commonly known as an advanced version of UV-NIL, which has the ability to fabricate nanostructures over an entire wafer in a short processing time. In S-FIL, the imprint material is a low-viscosity, photocurable monomer that is patterned using a transparent template. After the imprint material is dispensed dropwise on the substrate, the template is brought into close contact with the substrate. Due to the capillary action, the imprint material flows in the template pattern without the application of elevated temperature and pressure. The liquid monomer is then exposed to UV light through the transparent template, resulting in the photopolymerization and solidification of the imprinted features.

Typical resists used in S-FIL are either acrylate- or vinyl ether-based formulations.[31−35] The formulations usually have at least 9% silicon to obtain sufficient etch selectivity during the oxygen-reactive ion etch step. Acrylate-based resists are popular due to the easy availability of the monomers. Due to the difficulties associated with resist formulation with desired properties such as low viscosity, flowability, photocurability, and stability, S-FIL has not been so far used for direct patterning of functional materials such as oxides. TiO_2 has been chosen in our case to be patterned using S-FIL because of its extensive applications. Furthermore, the current patterning techniques used to pattern oxides suffer from the problem of low throughput. The problem of low throughput can be addressed by using S-FIL, which has the capability to pattern materials on wafer-scale.[36] In this paper, we show the first proof-of-concept of direct patterning of oxides, in particular TiO_2, using S-FIL. For a successful S-FIL of a functional oxide, apart from low viscosity, it is also important that the organic solvent in the resist is kept to near zero, as its evaporation would lead to clogging of the dispensing tip orifice and can also change the spreading characteristics of resist. We overcame this issue by using the resist consisting of an allyl-functionalized titanium complex mixed with reactive diluents. Furthermore, we show that the imprinted structures can be successfully converted to TiO_2 nanostructures by a post-heat-treatment step.

RESULTS AND DISCUSSION

The success of S-FIL of any metal oxide strongly depends upon the stability of the metal precursor in the imprint resist. Recent studies on metal methacrylates mixed with a cross-linker and subjected to *in situ* copolymerization during thermal NIL gave ∼100% yield over 2 cm × 1 cm areas. This approach was successfully able to demonstrate fabrication of various metal oxide patterns, such as those of TiO_2, ZrO_2, Fe_2O_3, Nb_2O_5, and Ta_2O_5.[11,20] The resists for patterning these oxides were prepared by reacting their respective metal alkoxides with methacrylic acid. The product, *i.e.*, metal methacrylate, dissolved in alcohol, gave a clear solution. This gave us a starting point to test titanium methcrylate as a potential precursor for patterning TiO_2 using S-FIL.

Titanium ethoxide (3 mmol) was reacted with methacrylic acid (12 mmol) to give dark brown colored titanium methacrylate with ethanol as the byproduct. The product mixture was subjected to reduced pressure in order to remove alcohol, as its presence leads to clogging of the dispensing tip and can change the spreading characteristics of the resist due to solvent evaporation. However, attempts to remove alcohol more often resulted in polymerization of titanium methacrylate, a result of the high reactivity of (meth)acrylates that is often difficult to control. Since the allyl-functionalized compounds are less reactive than acrylates, we formulated an allyl-functionalized titanium complex by reacting titanium ethoxide (3 mmol) with 3-butenoic acid (12 mmol). The solution instantly turned deep brown, forming titanium tetra-3-butenoate with ethanol as the byproduct. When ethanol was completely removed under low pressure from this allyl-functionalized complex, it yielded a stable brown solid. However, we found that for a neat drop-dispensable formulation, the optimum amount of ethanol to be removed from the allyl-functionalized titanium complex was about 60 ± 10 wt %. After removal of this amount of ethanol from the complex, the resultant product was a highly viscous, dark brown liquid, which was used as the metal oxide precursor for acrylate- and vinyl ether-based resist formulations for S-FIL.

To test the acrylate-based S-FIL resist formulation, a viscous dark brown allyl-functionalized titanium complex was mixed with reactive diluent isobutyl acrylate (4 mmol) and cross-linker ethylene glycol diacrylate (4 mmol) to achieve suitable viscosity for drop-dispensing (see Figure 1 for their chemical formulas). The total moles of reactive diluent and cross-linker were decided on the assumption that they ideally saturate *all* the double bonds of allyl-functionalized titanium complex during photopolymerization. Prior to S-FIL, 2 wt % of the photoinitiator and 2 wt % of fluorinated monomer were added to this formulation and purged with argon gas for 1 min to remove any dissolved oxygen. The components and their associated functions of this resist formulation are shown in Table 1. Figure 2 shows the schematic representation of the processing steps.

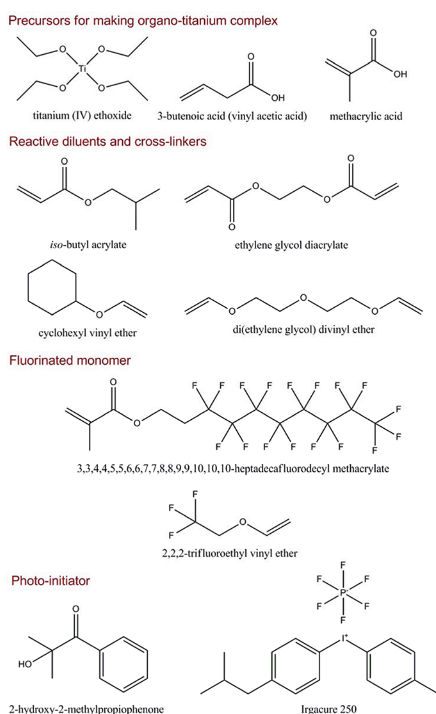

Figure 1. Listing of chemicals and their formulas used for the preparation of TiO_2 resist for S-FIL.

The final resist composition possessed a viscosity of ∼5 mPa·s, which is well within the limit (20 mPa·s) of the viscosity requirement for the S-FIL.[33] The TiO_2 S-FIL resist has a deep brown color (Figure 2, inset). Likewise, for the vinyl ether-based S-FIL resist formulation, a viscous dark brown allyl-functionalized titanium complex was mixed with reactive diluents di(ethylene glycol) divinyl ether (4 mmol) and cyclohexyl vinyl ether (4 mmol). To this were added 2 wt % of fluorinated monomer and 2 wt % of Irgacure 250, a photoacid generator. It was found that although this vinyl ether-based resist formulation possessed excellent low viscosity and was dispensable, it also resulted in clogging of the dispenser tip during S-FIL. This may be attributed to the presence of a small amount of unreacted 3-butenoic acid in the allyl-functionalized titanium complex that could spontaneously initiate the polymerization of vinyl ether monomers, thus reducing the shelf life of the resist dramatically. Consequently, only the acrylate-based S-FIL resist formulation was used for further studies.

To determine the experimental window of UV exposure during S-FIL, ultraviolet−visible (UV−vis) spectrophotometry was carried out on the acrylate-based TiO_2 resist. It is seen that the resist has steep UV absorption just below 340 nm wavelength. After UV curing, the absorption characteristic of the resist remains almost the same as that of the uncured resist except for a slight decrease in absorption below ∼270 nm (Figure 3a). Photo-DSC studies of the TiO_2 resist shows that it takes about 45 s to completely cure the resist in UV radiation (Figure 3b). The allyl-functionalized titanium complex is a highly light absorbing complex (dark brown color), and hence there is a loss of UV radiation due to absorption by the complex in the TiO_2 resist. This is confirmed by the fact that photo-DSC studies on photopolymerization of *only* the reactive diluent and cross-linker (*i.e.*, *sans* allyl-functionalized titanium complex) can be completed in ∼6 s. Therefore, during S-FIL, an extended time of UV exposure up to 2 min was used in order to ensure complete photopolymerization.

Figure 4 shows the FTIR analysis of the allyl-functionalized titanium complex and the acrylate-based TiO_2 resist formulation. Table 2 gives the assignments of the principal peaks.[37] The allyl-functionalized titanium complex showed characteristic peaks of a carbonyl group at 1716 cm^{-1}, a vinyl group at 1643 cm^{-1}, and a chelating carboxylate group at 1547 and 1410−1440 cm^{-1}. This confirmed the formation of the allyl-functionalized titanium complex. The IR spectrum of the TiO_2 S-FIL resist formulation exhibited the characteristic peaks of a carbonyl group at 1730 cm^{-1}, an *s-trans* acrylate double bond at 1640 cm^{-1}, an *s-cis* acrylate double bond at 1616 cm^{-1}, and a chelating carboxylate group at 1550 and 1410−1440 cm^{-1}. It can be seen that the vinyl group from the allyl-functionalized titanium complex has merged with the *s-trans* acrylate double bond. After a 2 min UV exposure, the C═C stretching peak has completely disappeared, while the peaks of C═O of the free and chelating carbonyl groups remain unchanged, suggesting the occurrence of UV-induced photopolymerization in this resist system. It is noteworthy that the metal−carbonyl chelation bond remains unaffected during the polymerization, thus keeping the metal atoms trapped inside the polymer network. This enables one to convert the structure to the corresponding metal oxide by post-imprinting heat-treatment.

An Imprio 100, from Molecular Imprints, Inc., was used to pattern the TiO_2 resist in two steps. First, the resist was deposited on a silicon wafer by direct drop-dispensing. The volume of drops was locally adjusted according to the pattern to be imprinted. After dispensing, the template containing 100 nm gratings (aspect ratio = 1) was pressed into the liquid monomer and held for 120 s at a pressure of 500 mbar to fill all of the features. Second, the imprint material was photopolymerized by broadband UV-light irradiation through the transparent template for 120 s, followed by demolding. The demolding forces were found to be in the range 5−10 N. This process was stepped and repeated five times, as seen in Figure 5a. The obtained yield was estimated optically to be >95%. Likewise, another quartz template containing composite features was used to imprint structures such as squares, dots, and lines, with different pattern densities, to test the ability of the TiO_2 resist to fill the mold uniformly.

TABLE 1. TiO_2 Resist Formulation for S-FIL and Description of Its Components

compound	weight %	function
titanium tetra-3-butenoate	48	metal oxide precursor, monomer; converts to metal oxide after heat-treatment
isobutyl acrylate	21	low-viscosity, reactive diluent; improves monomer flow
ethylene glycol diacrylate	27	cross-linker; improves mechanical properties
3,3,4,4,5,5,6,6,7,7,8,8,9,9,10,10,10-heptadecafluorodecyl methacrylate	2	fluorinated monomer; prevents sticking of resist to the mold by reducing its surface energy
2-hydroxy-2-methylpropiophenone	2	photoinitiator; generates free radicals upon exposure to UV radiation

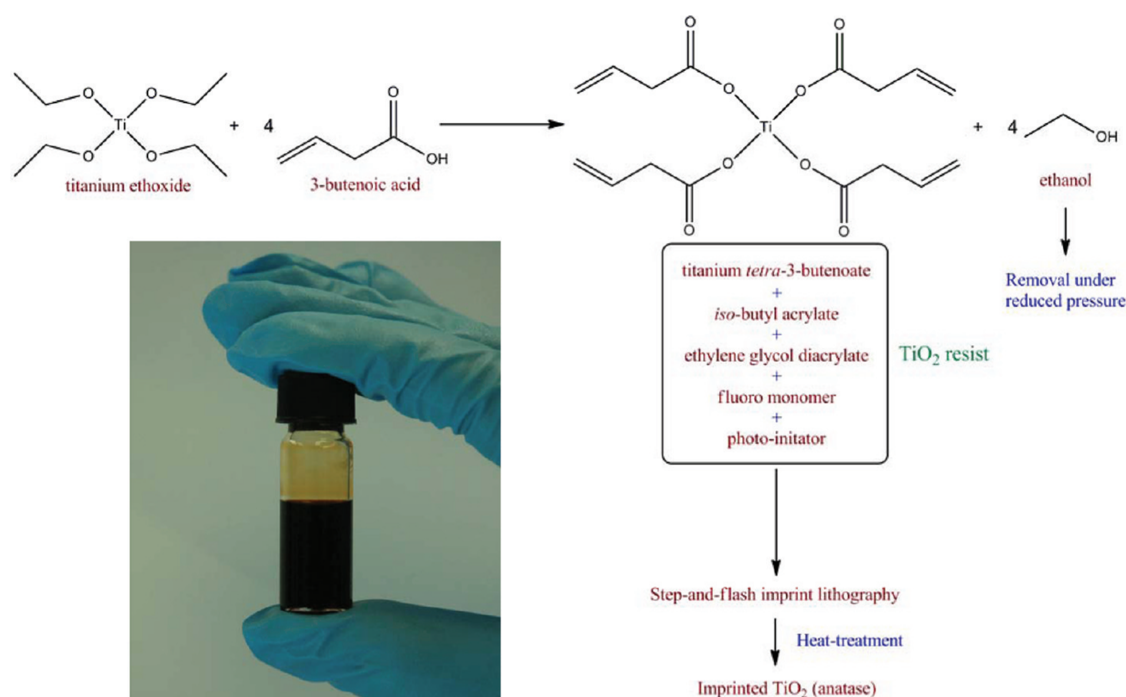

Figure 2. Schematic representation of process steps for direct imprinting of TiO_2 using S-FIL. Inset: Notice the dark brown color of the acrylate-based TiO_2 resist arising due to the allyl-functionalized titanium complex.

Cross-sectional scanning electron microscopy (SEM) studies show that the width and height of the imprinted features were slightly smaller than the actual dimensions of the mold, a result most likely due to the polymerization-induced shrinkage of the patterns. For example, 100 nm grating molds gave ~76 nm line-widths with a residual layer thickness of ~66 nm. On other hand, a 200 and 100 nm square and circular dimple containing template gave ~192 and ~90 nm feature sizes, respectively. Furthermore, it is seen that the features with different pattern densities can be simultaneously imprinted without any issues related to improper filling (Figure 5b and c), suggesting that the TiO_2 S-FIL resist formulation is insensitive to pattern density variations.

The photopolymerized TiO_2 resist was subjected to thermogravimetric analysis (TGA) in order to understand its mass loss behavior. The TGA shows two distinct regions of almost equal mass loss: a loss between 25 and 180 °C, which is most likely due to the decomposition of the allyl-functionalized titanium complex, and a further loss between 200 and 500 °C resulting from the loss of organic material from the resist, finally leading to 10.6% oxide residue (Figure 6a). This is in good agreement with the calculated value of ~10 wt %. X-ray diffraction (XRD) studies suggest that the anatase phase of TiO_2 can be obtained by heat-treating the resist film at 450 °C for 1 h (Figure 6b).

The imprinted patterns were heat-treated at 450 °C for 1 h in air to remove the organics and convert them to anatase. Atomic force microscopy (AFM) and SEM were used to analyze the topography and morphology of the heat-treated imprinted structures. Heat-treatment resulted in shrinkage of the imprinted grating patterns to approximately one-quarter of the original size while maintaining its original aspect ratio of ~1. Neither cracking nor delamination of the residual layer was observed after the heat-treatment (Figure 5a). On the other hand, squares and dots patterns show considerably less shrinkage than gratings. The former were shrunk by one-third of their original feature size. It is interesting to note that squares and dots patterns

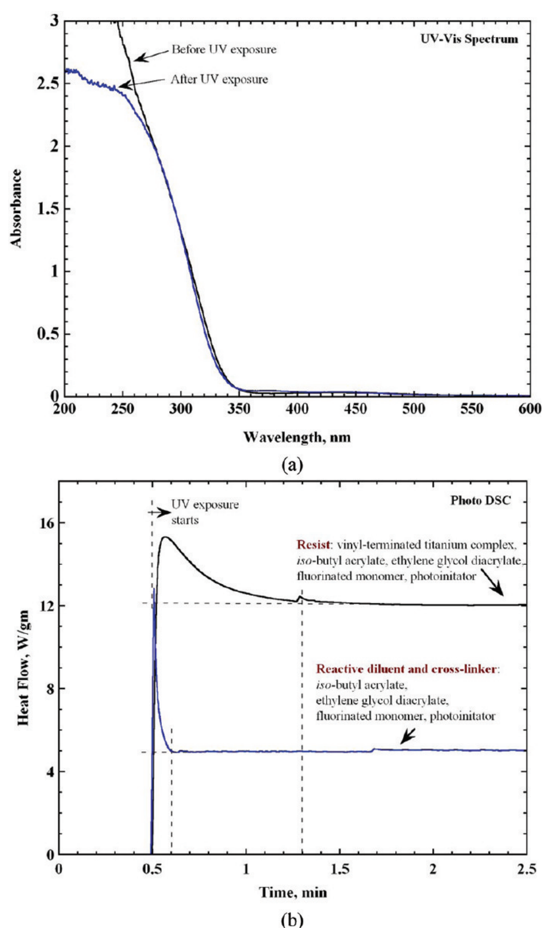

Figure 3. (a) UV–vis spectroscopy and (b) photo-DSC of acrylate-based TiO_2 resist for S-FIL. Notice that in (b), due to the deeply colored resist, the curing time in UV is higher.

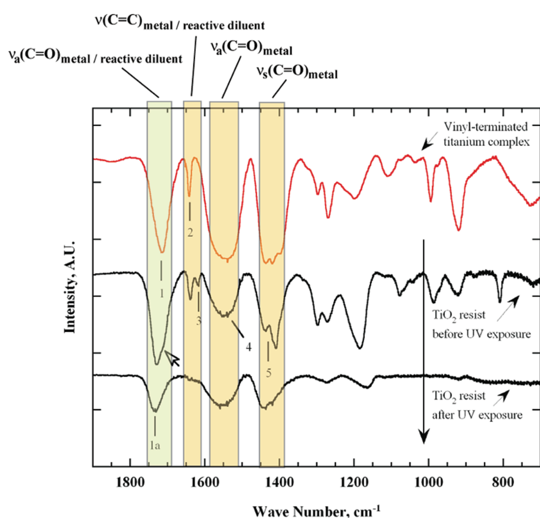

Figure 4. FTIR spectra of vinyl-terminated titanium complex and acrylate-based TiO_2 resist before and after UV exposure. The broad vibration bands corresponding to particular bonds are indicated on top. The arrow indicating a shoulder at 1716 cm^{-1} in the TiO_2 resist comes from the vinyl-terminated titanium complex. The principal peaks are identified in Table 2.

show a similar amount of shrinkage. This is not surprising, as similarly shaped features shrink to similar amounts when heat-treated. Our observation is also supported by proximate shrinkage values obtained for heat-treated 250 and 100 nm thermal nanoimprinted TiO_2 lines.[11] The AFM profile confirms that the heat-treatment-induced loss of the organic component occurred uniformly over the entire imprinted structure (Figure 5b and c and Table 3). In all cases, the center-to-center distance remains the same, while the edge-to-edge distance increases, clearly showing a slight decrease in feature density of heat-treated patterns. It must be emphasized that although the calcination shrinkage comes at the cost of pattern density, it is actually an easy way to access the nanoscale. It is one of the few techniques that benefit from the control imparted by top-down fabrication, yet the shrinkage can be thought of as a type of self-assembly and is bottom-up in nature. Thus here we have a hybrid approach toward fabrication of nanoscale oxide features. Furthermore, it has been noticed in the earlier studies that for a particular oxide resist composition, the degree of shrinkage can be predicted for gratings and other structures and, therefore, modeled in advance and incorporated into the mold geometry for precise control over critical dimensions.[11,20]

TABLE 2. Characteristic Infrared Absorption Peaks of Allyl-Functionalized Titanium Complex and Acrylate-Based TiO_2 Resist Showing Principal Peaks

absorption peak, cm^{-1}	assignment	peak number
1716	$\nu_a(C{=}O)_{metal\ complex}$	1
1730	$\nu_a(C{=}O)_{reactive\ diluent}$	1a
1643	$\nu(C{=}C)_{metal\ complex}$	2
1616	$\nu(C{=}C)_{reactive\ diluent}$	3
1550	$\nu_a(C{=}O)_{metal\ complex}$	4
1410–1440	$\nu_s(C{=}O)_{metal\ complex}$	5

The potential application of TiO_2 patterns, with or without the residual layer, produced by S-FIL depends ultimately on electrical, optical, and mechanical properties after heat-treatment. Residual layer thickness depends upon various factors, primary among them being the volume of individual resist drops used for drop-dispensing before S-FIL, the degree of flatness of the silicon wafer, and the accuracy of template alignment. A smaller volume of resist leads to lower residual layer thickness. Variations in the flatness of the silicon wafer as well as minor inaccuracies in template alignment also give rise to changes in the residual layer thickness within an imprint as well as from imprint to imprint. A two-probe instrument was used to carry out resistivity measurement on a 400 nm thin film that was formed by spin-coating and photopolymerization of a TiO_2 resist, followed by its thermal treatment at 450 °C for 1 h. The resistivity of the film was found to be about 2.3×10^2 Ω cm. This value is in line with the literature reports for polycrystalline TiO_2 thin films, which is in the range of 10^2 to 10^5 Ω cm.[38,39] The refractive index (*n*)

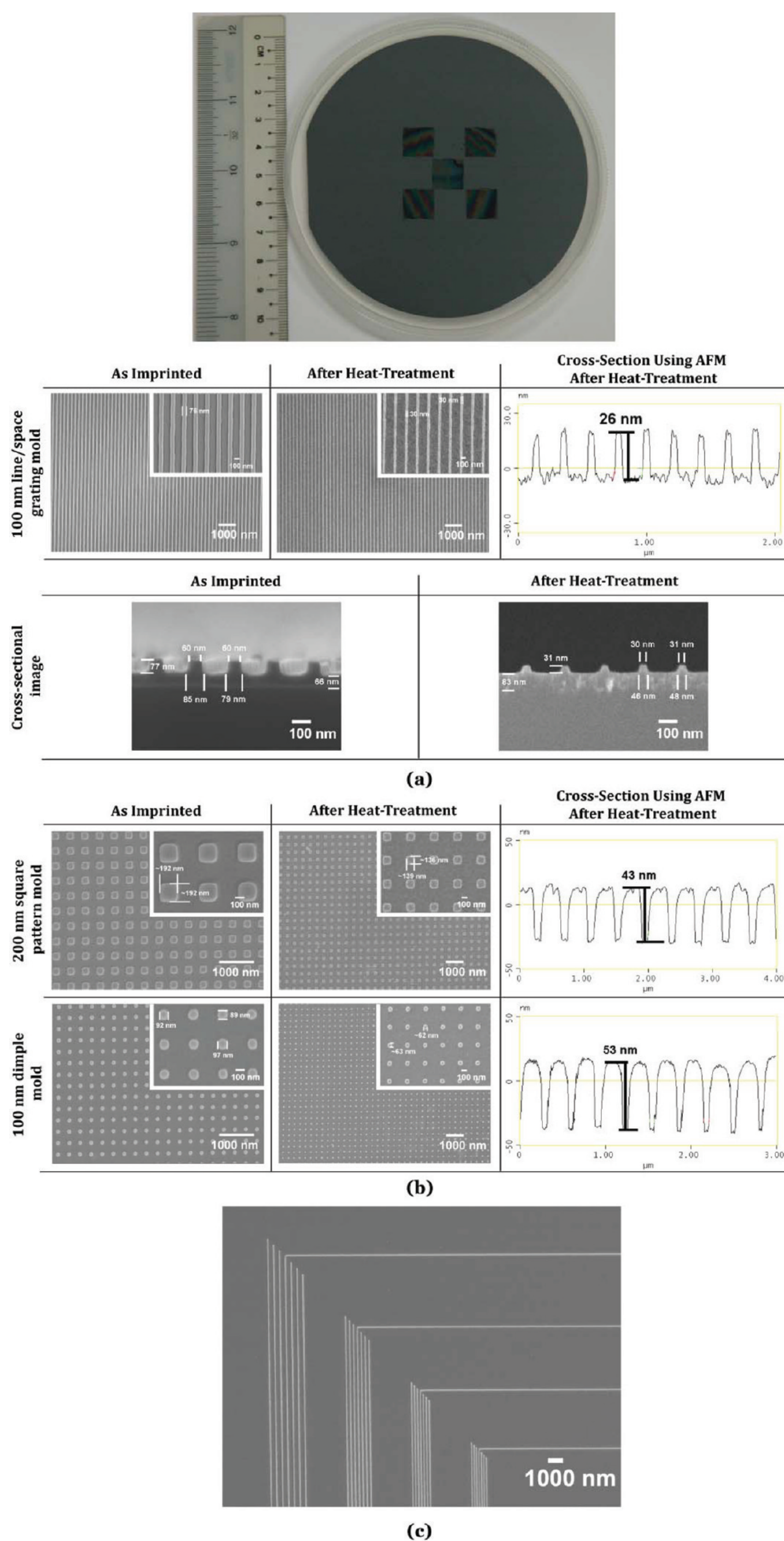

Figure 5. (a) Silicon wafer showing a five-field S-FIL of TiO_2 resist with a quartz template consisting of 100 nm line/space gratings over 1 cm × 1 cm area. Composite SEM images of as-imprinted and heat-treated structures of TiO_2 using this mold. The insets show the gratings at higher magnification. The AFM line traces of the corresponding heat-treated imprinted structures are shown on the right. Cross-sectional SEM image of the gratings before and after the heat-treatment shows the presence of a slight trapezoidal cross-section. Differences in the residual layer thickness within an imprint may arise from slight variations in the degree of flatness of the wafer and/or inaccuracies in template alignment. (b) Composite SEM images of square and dimple patterns and (c) 100 nm gratings with different line densities (right to left, pitch = 250, 200, 150, 100 nm) patterned using S-FIL of a TiO_2 resist, suggesting that the formulation is insensitive to pattern density variations.

of the TiO_2 anatase thin film was measured using ellipsometry, and the value was found to be 2.2 ± 0.02. This is very close to the reported value ($n = 2.3$) for TiO_2 thin films prepared by the sol–gel method[40] and compares well with the value associated with bulk TiO_2 ($n = 2.5$). An Agilent Nanoindenter G200 with DCM II option, equipped with a Berkovich tip, was used to test the modulus and hardness of TiO_2 films. The load was applied at a constant strain rate of 0.05 s^{-1} until the depth reached was 200 nm. The modulus and hardness data were extracted from a depth range of 8–10 nm.

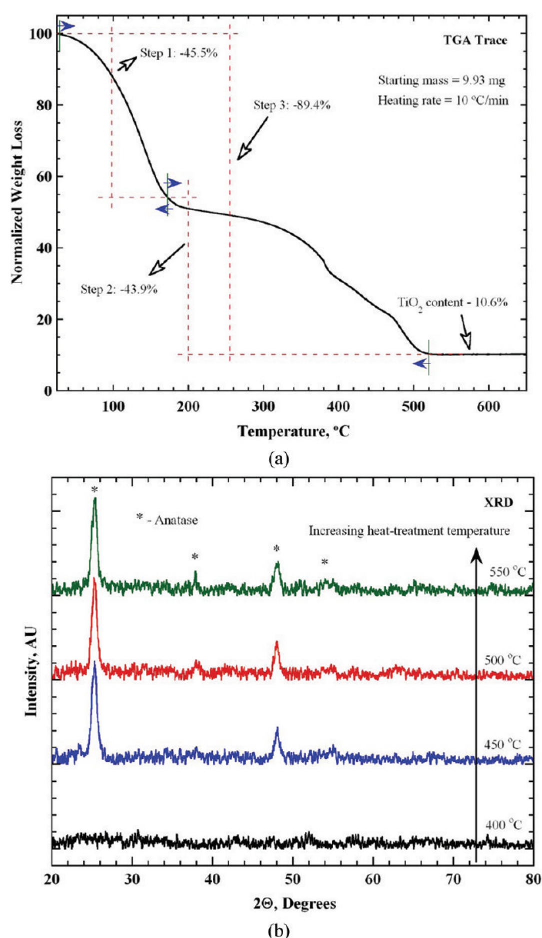

Figure 6. (a) TGA study of TiO_2 resist used for S-FIL. (b) XRD data of TiO_2 resist heat-treated at various temperatures for 1 h. Anatase phase appears at 450 °C, and its peaks are indicated by the * symbol.

The modulus and hardness of TiO_2 films heat-treated at 450 °C for 1 h were found to be 87.2 ± 7.9 and 4.51 ± 0.76 GPa, respectively. Heat-treating the films at 550 °C resulted in a slight increase in modulus (96.2 ± 11.9 GPa) and hardness (5.56 ± 1.06 GPa). This is most likely due to slightly denser packing of grains at higher temperature annealing. The hardness and modulus values are very similar to the literature reports of TiO_2 thin films fabricated by various techniques.[41−43]

From our discussion, it is clear that resist formulation based on an allyl-functionalized titanium complex and acrylate-based monomers offers numerous advantages for patterning TiO_2 using S-FIL. First, unlike its (meth)acrylate counterpart, the allyl-functionalized titanium complex is less reactive and hence relatively more stable at room temperature. This property gave a stable and low-viscosity resist formulation at room temperature. Second, the metal content in the resist can potentially be varied over a range of compositions without adversely affecting the dispensability, which may give rise to variable oxide pattern widths post-heat-treatment. Third, the resist formulation involves easily available and less-expensive monomers. This makes the commercial exploitation of the resist attractive. Fourth, our S-FIL technique, as opposed to conventional patterning methods, enables one to achieve large-area functional metal oxide nanostructures at a high throughput. Moreover, as metal oxides are generally hard materials, they can be directly used as imprint molds by exploiting the shrinkage to achieve high-resolution patterns. However, in those cases where one-to-one pattern replication is desired, the imprinted structures can be straight away used, as the metal-containing photopolymerized resist can act as an excellent etch mask. Fifth, calcination shrinkage of imprints enables the easy access of the nanoscale and is predictable given the resist composition and the type of feature. Therefore, it can be modeled in advance and incorporated into the template geometry for achieving control over critical dimensions. Lastly, our approach can easily be extended to fabricate functional nanostructures of other metal oxides as well. Furthermore, it may be possible to fabricate metal nanostructures by hydrogen reduction of metal

TABLE 3. Summary of the Approximate Feature Size Reduction at Every Step of the TiO_2 Patterning Using S-FIL

	feature size of the imprint after photopolymerization		oxide feature size after the heat-treatment of imprinted structures		
mold shape/size	width of imprint, nm	feature size reduction, %	width of the oxide feature, nm	feature size reduction, %	total feature size reduction with respect to mold feature size, %
lines, 100 nm	80	20%	30	63%	70%
square dimples, 200 nm	192	4%	136	29%	32%
round dimples, 100 nm	90	10%	62	31%	38%

oxides that reside above the water formation line in the Ellingham diagram.[44]

However, our resist does suffer from a drawback: its deep brown color results in loss of UV radiation due to absorption by the complex in the TiO_2 resist. This results in longer exposure time, thereby, adversely affecting the lifetime of the antisticking layer on the template surface. Such a concern may be alleviated by a slight change in chemistry of the titanium complex that can possibly result in an almost colorless resist formulation.

CONCLUSION

In conclusion, high-resolution, direct patterning of TiO_2 has been demonstrated with step-and-flash imprint lithography using a resist formulation based on the combination of an allyl-functionalized titanium complex and acrylate-based monomers. This TiO_2 resist formulation exhibits low enough viscosity to be dispensed by an automatic dispensing system and rapidly photopolymerized when subjected to broadband UV radiation through a transparent template. Moreover, this resist formulation was found to be insensitive to pattern density variations. Heat-treatment of the imprinted structures at 450 °C was accompanied by shrinkage without the loss of integrity or aspect ratio and their conversion to TiO_2 anatase nanostructures as small as 30 nm wide. This development could significantly advance nanoimprint technology, where fewer processing steps are needed to pattern a metal oxide on a wafer-scale. Our method is a facile and general route that may open a new way to achieve S-FIL of other functional oxides on the wafer-scale.

MATERIALS AND METHODS

Materials. To make and test resist formulations, chemicals such as titanium(IV) ethoxide (99.99% Ti, Strem Chemicals), 3-butenoic acid (Sigma Aldrich), methacrylic acid (Sigma Aldrich), isobutyl acrylate (Sigma Aldrich), ethylene glycol diacrylate (Sigma Aldrich), di(ethylene glycol) divinyl ether (Sigma Aldrich), cyclohexyl vinyl ether (Sigma Aldrich), 2,2,2-trifluoroethyl vinyl ether (Sigma Aldrich), and 3,3,4,4,5,5,6,6,7,7,8,8,9,9,10,10,10-heptadecafluorodecyl methacrylate (Sigma Aldrich) were used without any further purification. Irgacure 250, a photoacid generator, was obtained from Ciba, and 2-hydroxy-2-methylpropiophenone, a photoinitiator, was purchased from Sigma Aldrich.

Resist Formulation and Characterization. Titanium(IV) ethoxide was reacted with either methacrylic acid or 3-butenoic acid in a 1:4 molar ratio to form either methacrylate or an allyl-terminated metal complex with ethanol as the byproduct. A part or all of the alcohol was preferentially removed by subjecting the product to reduced pressure. To this, suitable reactive diluents were added depending upon acrylate- or vinyl ether-based formulations to result in a viscosity appropriate for drop-dispensing for subsequent S-FIL. For acrylate- and vinyl ether-based routes, a 2 wt % of 3,3,4,4,5,5,6,6,7,7,8,8,9,9,10,10,10-heptadecafluorodecyl methacrylate and 2,2,2-trifluoroethyl vinyl ether, both of them fluorinated monomers, were respectively added in order to reduce the surface energy of the imprinted resin to give clean template removal. Both acrylate- and vinyl ether-based formulations contained 2 wt % of photoinitiator or photoacid generator, respectively. All the formulations (*i.e.*, TiO_2 resists) were purged with argon gas for 2−3 min to remove dissolved oxygen.

Imprinting time for suitable resist formulations was determined using a photodifferential scanning calorimeter (p-DSC, TA Instruments Q100) equipped with a UV source (power: 300 mW cm^{-2}). A Nicolet 6700 Fourier transform infrared (FTIR) spectroscope was used to analyze the change in molecular structure of the resists before and after photopolymerization. Thermogravimetric analysis (TA Instruments Q500) was used to determine the degradation temperature of organic constituents and formation of TiO_2. This information was used for the heat-treatment of imprinted samples in a furnace heated at the rate of 10 °C min^{-1}.

Patterning Using S-FIL. All of the imprints were carried out on an Imprio 100 from Molecular Imprints, Inc. (USA). Double-sided, polished silicon wafers were used as substrates. Silicon wafers and quartz templates were cleaned using hot piranha solution (3:7 by volume of 30% H_2O_2 and H_2SO_4; *Warning: Piranha solution reacts violently with most organic materials and must be handled with extreme care!*) for 2 h to remove any surface organic contaminants, followed by washing with deionized water and blow drying using a nitrogen gun. After cleaning, the silicon wafers were spin-coated with a 2 nm thin layer of TranSpin (Molecular Imprints, Inc.), an adhesion promoter. Quartz templates were silanized with 1*H*,1*H*,2*H*,2*H*-perfluorodecyltrichlorosilane for 5 h to decrease their surface energy and to enable a clean demolding after imprinting.

Characterization of Imprints. Scanning electron and atomic force microscopies were used to study the topography and morphology of imprinted features before and after heat-treatment. A JEOL JSM6700F field-emission scanning electron microscope (FE-SEM) was used to acquire high-resolution images of as-imprinted as well as heat-treated imprinted structures. To find the height of the imprinted structures before and after heat-treatment, a Digital Instruments Nanoscope IV atomic force microscope was used. For X-ray diffraction analysis, the TiO_2 resist was spin-coated on a silicon substrate and photopolymerized using UV radiation, followed by heat-treatment at different temperatures. A Bruker D8 general area detector diffraction system equipped with a Cu Kα source was used for XRD analysis of heat-treated metal oxide films.

Acknowledgment. The authors would like to thank Shreya Kundu, L. P. Chong, and S. Lu of Institute of Materials Research and Engineering (IMRE) for their assistance in SEM, XRD, and hardness measurement, respectively. The help of Ms. B. Radha of the Jawaharlal Nehru Centre for Advanced Scientific Research, Bangalore (India), in electrical conductivity measurements is gratefully acknowledged. This work was supported by the IMRE-funded core project no. IMRE/09-1C0319.

REFERENCES AND NOTES

1. Shi, J.; Sun, C.; Starr, M. B.; Wang, X. Growth of Titanium Dioxide Nanorods in 3D-Confined Spaces. *Nano Lett.* **2011**, *11*, 624–631.
2. Que, W.; Zhou, Y.; Lam, Y. L.; Kam, C. H. Preparation and Characterizations of $SiO_2/TiO_2/\gamma$-Glycidoxypropyltrimethoxysilane Composite Materials for Optical Waveguides. *Appl. Phys. A: Mater. Sci. Process.* **2001**, *73*, 171–176.
3. Fujishima, A.; Rao, T. N.; Tryk, D. A. Titanium Dioxide Photocatalysis. *J. Photochem. Photobiol. C* **2000**, *1*, 1–21.
4. Smetaniuk, D. P.; Taschuk, M. T.; Brett, M. J. Photocatalytic Titanium Dioxide Nanostructures for Self-Regenerating Relative Humidity Sensors. *IEEE Sens. J.* **2011**, *11*, 1713–1719.

5. Tohge, N.; Shinmou, K.; Minami, T. Characteristics of Diffraction Gratings Fabricated by the Two-Beam Interference Method Using Photosensitive Hybrid Gel Films. *J. Sol-Gel Sci. Technol.* **2000**, *19*, 119–123.
6. Saifullah, M. S. M.; Subramanian, K. R. V.; Tapley, E; Kang, D. J.; Welland, M. E.; Butler, M. Sub-10 nm Electron Beam Nanolithography Using Spin-Coatable TiO_2 Resists. *Nano Lett.* **2003**, *3*, 1587–1591.
7. Duoss, E. B.; Twardowski, M.; Lewis, J. A. Sol-Gel Inks for Direct-Write Assembly of Functional Oxides. *Adv. Mater.* **2007**, *19*, 3485–3489.
8. Passinger, S.; Saifullah, M. S. M.; Reinhardt, C.; Subramanian, K. R. V.; Chichkov, B. N.; Welland, M. E. Direct 3D Patterning of TiO_2 Using Femtosecond Laser Pulses. *Adv. Mater.* **2007**, *19*, 1218–1221.
9. Voicu, N. E.; Saifullah, M. S. M.; Subramanian, K. R. V.; Welland, M. E.; Steiner, U. TiO_2 Patterning Using Electro-Hydrodynamic Lithography. *Soft Matter* **2007**, *3*, 554–557.
10. Van Kan, J. A.; Bettiol, A. A.; Chiam, S. Y.; Saifullah, M. S. M.; Subramanian, K. R. V.; Welland, M. E.; Watt, F. New Resists for Proton Beam Writing. *Nucl. Instrum. Methods Phys. Res., Sect. B* **2007**, *260*, 460–463.
11. Lim, S. H.; Saifullah, M. S. M.; Hussain, H.; Loh, W. W.; Low, H. Y. Direct Imprinting of High Resolution TiO_2 Nanostructures. *Nanotechnology* **2010**, *21*, 285303.
12. Park, H. H.; Choi, D. G.; Zhang, X.; Jeon, S.; Park, S. J.; Lee, S. W.; Kim, S.; Kim, K. D.; Choi, J. H.; Lee, J.; *et al.* Photo-Induced Hybrid Nanopatterning of Titanium Dioxide *via* Direct Imprint Lithography. *J. Mater. Chem.* **2010**, *20*, 1921–1926.
13. Schrift, H. Nanoimprint Lithography: An Old Story in Modern Times? A Review. *J. Vac. Sci. Technol. B* **2008**, *26*, 458–480.
14. Costner, E. A.; Lin, M. W.; Jen, W.-L.; Willson, C. G. Nanoimprint Lithography Materials Development for Semiconductor Device Fabrication. *Annu. Rev. Mater. Res.* **2009**, *39*, 155–180.
15. Guo, L. J. Nanoimprint Lithography: Methods and Material Requirements. *Adv. Mater.* **2007**, *19*, 495–513.
16. Chou, S. Y.; Krauss, P. R.; Renstrom, P. J. Nanoimprint Lithography. *J. Vac. Sci. Technol. B* **1996**, *14*, 4129–4133.
17. Austin, M. D.; Ge, H.; Wu, W.; Li, M.; Yu, Z.; Wasserman, D.; Lyon, S. A.; Chou, S. Y. Fabrication of 5 nm Linewidth and 14 nm Pitch Features by Nanoimprint Lithography. *Appl. Phys. Lett.* **2004**, *84*, 5299–5301.
18. Austin, M. D.; Zhang, W.; Ge, H.; Wasserman, D.; Lyon, S. A.; Chou, S. Y. 6 nm Half-Pitch Lines and 0.04 μm^2 Static Random Access Memory Patterns by Nanoimprint Lithography. *Nanotechnology* **2005**, *16*, 1058–1061.
19. Hua, F.; Sun, Y.; Gaur, A.; Meiti, M. A.; Bilhaunt, L.; Rotkina, L.; Wang, J.; Geil, P.; Shim, M.; Rogers, J. A. Polymer Imprint Lithography with Molecular-Scale Resolution. *Nano Lett.* **2004**, *4*, 2467–2471.
20. Ganesan, R.; Lim, S. H.; Saifullah, M. S. M.; Hussain, H.; Kwok, J. X. Q.; Tse, R. L. X.; Bo, H. A. P.; Low, H. Y. Direct Nanoimprinting of Metal Oxides By *in Situ* Thermal Co-Polymerization of Their Methacrylates. *J. Mater. Chem.* **2011**, *21*, 4484–4492.
21. Li, M.; Tan, H.; Chen, L.; Wang, J.; Chou, S. Y. Large Area Direct Nanoimprinting of SiO_2-TiO_2 Gel Gratings for Optical Applications. *J. Vac. Sci. Technol. B* **2003**, *21*, 660–663.
22. Matsui, S.; Igaku, Y.; Ishigaki, H.; Fujita, J.; Ishida, M.; Ochiai, Y.; Namatsu, H.; Komuro, M. Room-Temperature Nanoimprint and Nanotransfer Printing Using Hydrogen Silsequioxane. *J. Vac. Sci. Technol. B* **2003**, *21*, 688–692.
23. Kim, W. S.; Yoon, K. B.; Bae, B. S. Nanopatterning of Photonic Crystals with a Photocurable Silica−Titania Organic−Inorganic Hybrid Material by a UV-Based Nanoimprint Technique. *J. Mater. Chem.* **2005**, *15*, 4535–4539.
24. Göbel, O. F.; Nedelcu, M.; Steiner, U. Soft Lithography of Ceramic Patterns. *Adv. Funct. Mater.* **2007**, *17*, 1131–1136.
25. Kwon, S. J.; Park, J. H.; Park, J. G. Selective Growth of ZnO Nanorods by Patterning of Sol-Gel-Derived Thin Film. *J. Electroceram.* **2006**, *17*, 455–459.
26. Hampton, M. J.; Williams, S. S.; Zhou, Z.; Nunes, J.; Ko, D. H.; Templeton, J. L.; Samulski, E. T.; DeSimone, J. M. The Patterning of Sub-500 nm Inorganic Oxide Structures. *Adv. Mater.* **2008**, *20*, 2667–2673.
27. Yang, K.-Y.; Yoon, K.-M.; Choi, K. W.; Lee, H. The Direct Nano-Patterning of ZnO Using Nanoimprint Lithography with ZnO-Sol and Thermal Annealing. *Microelectron. Eng.* **2009**, *86*, 2228–2231.
28. Yang, K.-Y.; Yoon, K.-M.; Lim, S.; Lee, H. Direct Indium Tin Oxide Patterning Using Thermal Nanoimprint Lithography for Highly Efficient Optoelectronic Devices. *J. Vac. Sci. Technol. B* **2009**, *27*, 2786–2789.
29. Yoon, K.-M.; Yang, K.-Y.; Lee, H.; Kim, H.-S. Formation of TiO_2 Nanopattern Using Reverse Imprinting and Sol-Gel Method. *J. Vac. Sci. Technol. B* **2009**, *27*, 2810–2813.
30. Han, H.; Bhushan, A.; Yaghmaie, F.; Davis, C. E. Direct Thermal-UV Nanoimprint of an Iron-Containing Organometallic Hybrid Film. *J. Vac. Sci. Technol. B* **2010**, *28*, 78–81.
31. Long, B. K.; Keitz, B. K.; Willson, C. G. Materials for Step and Flash Imprint Lithography (S-FIL®). *J. Mater. Chem.* **2007**, *17*, 3575–3580.
32. Kim, E. K.; Stacey, N. A.; Smith, B. J.; Dickey, M. D.; Johnson, S. C.; Trinque, B. C.; Willson, C. G. Vinyl Ethers in Ultraviolet Curable Formulations for Step and Flash Imprint Lithography. *J. Vac. Sci. Technol. B* **2004**, *22*, 131–135.
33. Palmieri, F.; Adams, J.; Long, B.; Heath, W.; Tsiartas, P.; Willson, C. G. Design of Reversible Cross-Linkers for Step and Flash Imprint Lithography Imprint Resists. *ACS Nano* **2007**, *1*, 307–312.
34. Heath, W. H.; Palmieri, F.; Adams, J. R.; Long, B. K.; Chute, J.; Holcombe, T. W.; Zieren, S.; Truitt, M. J.; White, J. L.; Willson, C. G. Degradable Cross-Linkers and Strippable Imaging Materials for Step-and-Flash Imprint Lithography. *Macromolecules* **2008**, *41*, 719–726.
35. Takei, S. Step and Flash Imprint of Fluorinated Silicon-Containing Resist Materials for Three-Dimensional Nanofabrication. *Jpn. J. Appl. Phys.* **2010**, *49*, 071602.
36. Resnick, D. J.; Sreenivasan, S. V.; Willson, C. G. Step & Flash Imprint Lithography. *Mater. Today* **2005**, *8*, 34–42.
37. Nyquist, R. A.; Streck, R. Infrared Solution Study of Alkyl Acrylates and Alkyl Methacrylates in $CHCl_3$ and/or CCl_4 solutions. *Vib. Spectrosc.* **1994**, *8*, 71–85.
38. Tighineanu, A.; Ruff, T.; Albu, S.; Hahn, R.; Schmuki, P. Conductivity of TiO_2 Nanotubes: Influence of Annealing Time and Temperature. *Chem. Phys. Lett.* **2010**, *494*, 260–263.
39. Pomoni, K.; Vomvas, A.; Trapalis, C. Electrical Conductivity and Photoconductivity Studies of TiO_2 Sol−Gel Thin Films and the Effect of n-Doping. *J. Non-Cryst. Solids* **2008**, *354*, 4448–4457.
40. Wang, Z.; Helmersson, U.; Käll, P. O. Optical Properties of Anatase TiO_2 Thin Films Prepared by Aqueous Sol−Gel Process at Low Temperature. *Thin Solid Films* **2002**, *405*, 50–54.
41. Gaillard, Y.; Rico, V. J.; Pique, E. J.; Elipe, A. R. G. Nanoindentation of TiO_2 Thin Films with Different Microstructures. *J. Phys. D: Appl. Phys.* **2009**, *42*, 145305.
42. Mathur, S.; Kuhn, P. CVD of Titanium Oxide Coatings: Comparative Evaluation of Thermal and Plasma Assisted Processes. *Surf. Coat. Technol.* **2006**, *201*, 807–814.
43. Yaghoubi, H.; Taghavinia, N.; Alamdari, E. K.; Volinsky, A. A. Nanomechanical Properties of TiO_2 Granular Thin Films. *ACS Appl. Mater. Interfaces* **2010**, *2*, 2629–2636.
44. Nedelcu, M.; Saifullah, M. S. M.; Hasko, D. G.; Jang, A.; Anderson, D.; Huck, W. T. S.; Jones, G. A. C.; Welland, M. E.; Kang, D. J.; Steiner, U. Fabrication of Sub-10 nm Metallic Lines of Low Line-Width Roughness by Hydrogen Reduction of Patterned Metal-Organic Materials. *Adv. Funct. Mater.* **2010**, *20*, 2317–2323.